Earth Planets Space, **58**, 359–370, 2006

The *Swarm* End-to-End mission simulator study: A demonstration of separating the various contributions to Earth's magnetic field using synthetic data

Nils Olsen[1], Roger Haagmans[2], Terence J. Sabaka[3], Alexei Kuvshinov[1], Stefan Maus[4], Michael E. Purucker[3], Martin Rother[5], Vincent Lesur[6], and Mioara Mandea[5,7]

[1]*Danish National Space Center, Juliane Maries Vej 30, DK-2100 Copenhagen, Denmark*
[2]*Directorate of Earth Observation Programmes, ESTEC/ESA, Postbus 299, NL-2200 AG Noordwijk ZH, The Netherlands*
[3]*Geodynamics Branch, GSFC/NASA, Greenbelt, MD 20771, U.S.A.*
[4]*National Geophysical Data Center, NOAA, Boulder, CO 80305-3328, U.S.A.*
[5]*GFZ Potsdam, Telegrafenberg, D-14473 Potsdam, Germany*
[6]*British Geological Survey, Murchison House, West Mains Road, Edinburgh EH9 3LA, Scotland*
[7]*Institut de Physique du Globe de Paris, 4, Place Jussieu, B89, Tour 24, F-75252 Paris cedex 054, France*

(Received November 19, 2004; Revised June 20, 2005; Accepted June 22, 2005; Online published April 14, 2006)

Swarm, a satellite constellation to measure Earth's magnetic field with unpreceded accuracy, has been selected by ESA for launch in 2009. The mission will provide the best ever survey of the geomagnetic field and its temporal evolution, in order to gain new insights into the Earth system by improving our understanding of the Earth's interior and climate. An End-to-End mission performance simulation was carried out during Phase A of the mission, with the aim of analyzing the key system requirements, particularly with respect to the number of *Swarm* satellites and their orbits related to the science objectives of *Swarm*. In order to be able to use realistic parameters of the Earth's environment, the mission simulation starts at January 1, 1997 and lasts until re-entry of the lower satellites five years later. Synthetic magnetic field values were generated for all relevant contributions to Earth's magnetic field: core and lithospheric fields, fields due to currents in the ionosphere and magnetosphere, due to their secondary, induced, currents in the oceans, lithosphere and mantle, and fields due to currents coupling the ionosphere and magnetosphere. Several independent methods were applied to the synthetic data to analyze various aspects of field recovery in relation to different number of satellites, different constellations and realistic noise sources. This paper gives an overview of the study activities, describes the generation of the synthetic data, and assesses the obtained results.

Key words: Earth's magnetic field, comprehensive inversion, electromagnetic induction, ionosphere, lithosphere, magnetosphere.

1. Introduction

Swarm, a satellite constellation to study the dynamics of the Earth's magnetic field and its interactions with the Earth system (Friis-Christensen *et al*., 2006), has been selected by ESA for full implementation and launch in 2009. The objective of the *Swarm* mission is to provide the best ever survey of the geomagnetic field and its temporal evolution, in order to gain new insights into the Earth system by improving our understanding of the Earth's interior and climate.

High-precision and high-resolution measurements of the strength, direction and variation of the magnetic field, complemented by precise navigation, accelerometer and electric field measurements, will provide the necessary observations that are required to separate and model various sources of the geomagnetic field. This results in a unique view inside the Earth from space to study the composition and processes in the interior. It also allows the analysis of the Sun's influence within the Earth system. In addition, practical applications in many different areas, such as space weather, radiation hazards, navigation and resource exploration, benefit from the *Swarm* concept.

During Phase A of the mission, in 2003–2004, several studies were performed: In addition and in parallel to *system performance* simulations done by two industrial consortia, an End-to-End *mission performance* simulation (Olsen *et al*., 2004) has been carried out. The purpose of this simulator was to build a virtual (simulated) mission of the external environment (magnetic and electric fields), of the environmental disturbances on the spacecraft, and on the dynamics of the spacecrafts (orbit and attitude), with the aim of analyzing the key system requirements, particularly with respect to the number of *Swarm* satellites and their orbits related to the science objectives of *Swarm*. This paper gives an overview of the study activities, describes the generation of the synthetic data, and assesses the obtained results. For this assessment we focus on the primary research objectives of the *Swarm* mission: determination of the high-degree lithospheric field, of the core field and secular variation, and of 3D mantle conductivity.

The five-year full mission simulation starts one solar cy-

Copyright © The Society of Geomagnetism and Earth, Planetary and Space Sciences (SGEPSS); The Seismological Society of Japan; The Volcanological Society of Japan; The Geodetic Society of Japan; The Japanese Society for Planetary Sciences; TERRAPUB.

cle (11 years) before launch, which was scheduled for 2008 at the beginning of Phase A (i.e., the simulation starts at January 1, 1997, and lasts until re-entry of the lower satellites, which turned out to be about 5 years later), in order to use realistic indices of the Earth's environment. Synthetic magnetic field values were generated based upon a combination of existing and simulated synthetic models for all relevant contributions to Earth's magnetic field: core and lithospheric fields, fields due to currents in the ionosphere and magnetosphere, due to their secondary, induced, currents in the oceans, lithosphere and mantle, and fields due to currents coupling the ionosphere and magnetosphere.

Several independent methods were applied to the synthetic data to analyze various aspects of field recovery in relation to different numbers of satellites, different constellations and realistic noise sources. The comprehensive inversion (Sabaka *et al*., 2002, 2004), which contains parameterization of all relevant sources, has been chosen as the primary approach for field recovery and error analysis; the obtained results are described in detail in Sabaka and Olsen (2006). In addition, independent approaches for improved recovery of the lithospheric field, of field-aligned currents, and of mantle conductivity (Maus *et al*., 2006; Ritter and Lühr, 2006; Kuvshinov *et al*., 2006) show potential for further exploitation of the mission.

2. Forward Scheme: Production of Synthetic Data

2.1 Constellation design and generation of synthetic orbits

To obtain greater flexibility in the assessment of favorable constellations a pool of data and errors for a total of five different satellites were generated for the complete mission lifetime (5 years, 190 million satellite positions at 5 sec sampling rate), which amounted to 10,950 daily files (2.42 Mb each) per constellation run. Out of these five satellites, different constellations of 1, 2, 3 and 4 satellites were selected and the success of recovering the original models was analyzed for each constellation.

Orbital parameters of the various satellites were primarily those of the original proposal (Friis-Christensen *et al*., 2002), but with modifications based on the experience gained during the initial stage of the study: A major change in concept is to have two spacecraft flying side-by-side separated in East-West direction instead of two satellites following each other in the same orbital plane. This allows for the first time for a measurement of the East-West gradient of Earth's magnetic field (cf. Friis-Christensen *et al*. (2006) for a discussion of the advantages of gradient information). Also, orbit inclination has been increased slightly in order to reduce the size of the polar gaps (i.e. the regions close to the geographic poles that are not sampled by the satellites). Finally, the initial altitude was adjusted according to the present best guesses of spacecraft properties like mass and cross-section area, as resulting from the two industrial studies. In the following we will only present results for the constellation that was found to be most promising in terms of scientific return.

The satellites are in near-polar circular orbits at lower or higher altitude, and as individual or pair of satellites. The lower pair is dedicated to support the high-degree lithospheric magnetization studies and thus calls for a small separation, chosen in the study to be 1.5° in longitude. Table 1 lists the Kepler elements for the five satellites that are discussed in this paper, and Fig. 1 shows schematically the three-satellite constellation that has been finally selected (Data from two additional satellites, not shown in the Figure, have been used in the simulation study: *Swarm D* is located almost antipodal to *Swarm C* at the same altitude, but in an orbit plane that is shifted compared to *Swarm C* by 12° in longitude, and *Swarm E* is flying side-by-side to *Swarm D* in the same orbit plane as *Swarm C*.)

Generation of synthetic orbits has been performed by numerical integration of the equations of motion as they are programmed in the EPOS (Earth Parameter & Orbit System) software developed by GFZ Potsdam. The left part of Fig. 2 shows the obtained orbital decay, which is almost identical for spacecrafts at the same initial altitude. (Note that we used 550 km as initial altitude of the higher satellites C, D, and E. Since this altitude results in inconvienient repeat-tracks, a slightly lower altitude of 530 km will be used for the implementation of Swarm.) In order to obtain a separation between the orbital planes, the upper and lower spacecraft have been given a slightly different inclination. The precession of the orbital planes of the upper and lower satellites (i.e., the local time of the equator crossing of the north-going part of the orbit) is shown in the right part of the Figure. The drift rate of the lower satellites is slightly faster, which results in a local time difference of 6 hours after 36 months.

2.2 Description of the forward models

We used the 4th generation of the *Comprehensive Model*, CM4, (Sabaka *et al*., 2004) as the basic model for generating the synthetic data. This model provides the magnetic field contribution from the core (up to spherical harmonic degree/order $n = 13$), lithosphere (static field, up to $n = 65$), ionosphere, magnetosphere, from coupling currents (coupling the ionosphere and magnetosphere) and from secondary, Earth-induced contributions. However, some parts of the model have been modified: high-degree lithospheric field and secular variation models have been added, and the models of magnetospheric and induced fields have been replaced by more realistic ones. In the following we briefly describe the various parts of the augmented model.

Lithospheric field model

Since determination of the lithospheric field at spherical harmonic degrees higher than those of present models (reliable estimates exist only for $n < 60$ or so) is one of the main objectives of *Swarm*, we have to rely on hypothetical, but realistic, models of the high-degree lithospheric field. Two models have been derived for this purpose. Their low-degree part ($n \leq 30$) is identical; however, they differ in the way the high-degree part was designed.

The first model, swarm(11a/03), was found as following: The coefficients g_n^m, h_n^m for the lowest degrees (up to $n = 40$) are taken from CM4. Medium degree coefficients ($n = 40$–70) are taken from the field model MF2 derived by Maus *et al*. (see Maus *et al*. (2002) and www.gfz-potsdam.de/pb2/pb23/SatMag/litmod2.html); a cosine bell

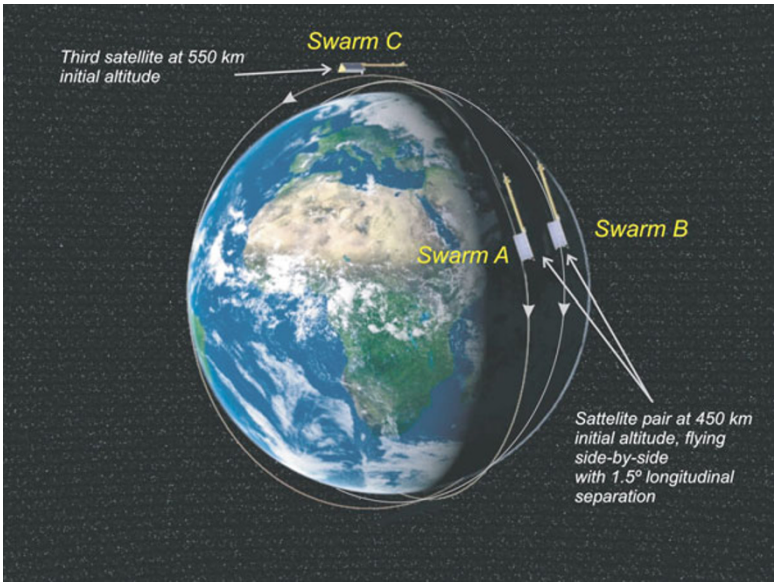


Fig. 1. Definition of the *Swarm* three-satellite constellation.

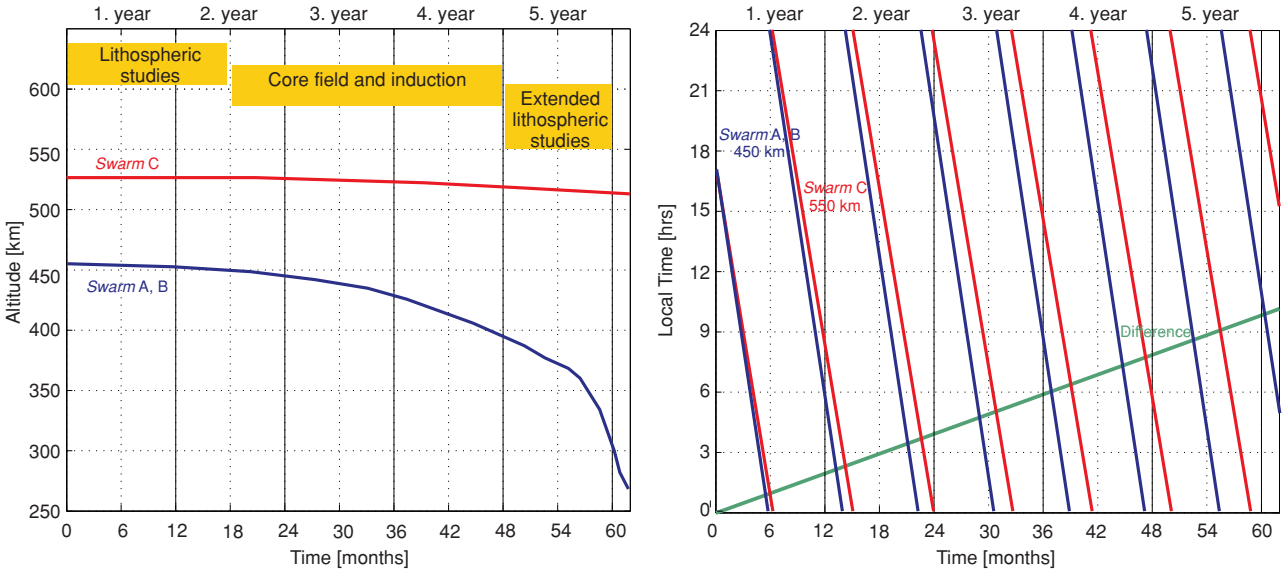


Fig. 2. Orbit evolution of the higher and lower satellites. Left: Orbital decay of the higher and lower satellites. Right: Precession of the orbital planes through local time. The lower satellites, *Swarm A,B*, drift slightly faster.

filter has been applied in order to obtain a smooth transition for coefficients between degree 35 and 45. The high degree coefficients ($n = 71$–120) are taken from a synthetic model, based on an extrapolation of the MF2 spectrum (linear fit to $\log(R_n)$ for $n = 25$–70, where R_n is the Mauersberger-Lowes spectrum) and assuming that the amplitudes of all coefficients for a given n are from a common Gaussian distribution. This approach is similar to the one used for generating a synthetic model of the gravity field (Haagmans, 2000). Coefficients with $n > 110$ are tapered to zero at $n = 120$. Power spectra of the merged model, swarm(11a/03), together with that of its constituents, is shown in Fig. 3.

During the study it was recognized that a lower pair of satellites flying side-by-side with longitudinal separation of 1.5° (corresponding to about 170 km at the Equator) would probably allow for determination of the lithospheric at degrees higher ($n > 110$) than that provided by the first model. To test this, a second synthetic lithospheric model, swarm(06a/04), was designed, with maximum degree and order of $n = 150$. Contrary to the first model, which is designed from the expected statistical properties of the high-degree lithospheric field, this second model is based on models of remanent and induced magnetization. We begin with a 1/2 degree grid of vertically integrated remanent magnetization developed by Dyment and Arkani-Hamed (1998) for the oceanic crust based on an age map of the oceans, the relative motion of the plates, and the African Apparent Polar Wander Path. Neither satellite, shipborne, or aeromagnetic data were used in this initial compilation. However, the grid was calibrated against observations of the satellite anomaly field in the North Atlantic, and sub-

Table 1. Kepler elements for epoch January 1, 1997, 00:00 UT (launch). Zero eccentricity, i.e. circular orbits, for all satellites (cf. Seeber, 2004) for an explanation of *RAAN (= Right ascension of the ascending node), mean anomaly, inclination*, and *nodal drift rate*). $a = 6371.2$ km is the reference radius for the altitude.

	Altitude	RAAN	Mean anomaly	Inclination	Nodal drift rate
Swarm A	450 km	0°	0°	86.8°	−0.4397°/day
Swarm B	450 km	−1.5°	0°	86.8°	−0.4397°/day
Swarm C	550 km	0°	90°	87.3°	−0.3526°/day
Swarm D	550 km	−12°	270°	87.3°	−0.3526°/day
Swarm E	550 km	0°	270°	87.3°	−0.3526°/day

sequently, in the South Atlantic (Purucker and Dyment, 2000). Because the magnetization grid is not global, and continental crust is assigned a zero magnetization, ringing is a problem.

To suppress this ringing we added a model of induced magnetization to the oceanic remanent magnetization. This induced magnetization model is based on 11562 dipoles located on an icosahedral tesselation, with an average spacing of 1.89° (210 km), the current version of which is documented in Fox Maule *et al.* (2005). The model is determined by iteration from a starting model defined by the crustal thickness and heat flow of the seismic tomography model 3SMAC (Nataf and Ricard, 1996). After three iterations, residuals with respect to the MF-3 model (Maus *et al.*, 2005) are generally less than 1 nT. (The oceanic remanent model had first been removed from MF3 prior to this iterative process.). This crustal thickness model is then converted to an depth-integrated induced magnetization and added vectorially to the oceanic remanent magnetization model.

Next, a spherical harmonic expansion of the gridded magnetization distribution is performed, and the obtained spherical harmonic coefficients are recast in terms of Gauss coefficients g_n^m and h_n^m of the magnetic potential V. The procedures have been detailed in appendix A of Dyment and Arkani-Hamed (1998). Power spectra of the models are shown in Fig. 3. The obtained model, called COAP199, has less power than MF3, and hence has been scaled by a factor of 1.4 to bring its power in the degree range between $n = 20$ and 80 to the same level as model MF-3; the scaled model is called swarm(06a/04). Coefficients for $n < 30$ are taken from CM4.

The induced and remanent magnetization models do not fit seamlessly together, as shown by the dip in the spectra near degree 90. The induced magnetization model is considerably less detailed than the remanent model, and we believe that this dip is a manifestation of that difference in detail between the models.

Figure 4 shows the lithospheric radial magnetic component at ground derived from MF-3 up to degree 60, left panel, and the improvement (field models up to degree 130) that *Swarm* will provide, right panel. This improvement will bridge the existing gap between satellite models and data from ground, airborne and marine surveys.

Secular variation model The core field coefficients are those given by CM4 for $n \leq 10$; their temporal behavior is described by cubic splines with a knot separation of 2.5 years. Secular variation for $n = 11 - 19$ is assumed to be linear and created from a fitted spectrum in the same way as described above for the lithospheric field; the spectrum was that of model oersted (10a/03) (cf. www.spacecenter.dk.dk/projects/oersted/models/) derived using data from the Ørsted and CHAMP satellites.

Conductivity model of the Earth A model of the electrical conductivity of the Earth, including the conductivity of the seawater and of some inhomogeneities in the deep mantle, is required to generate realistic induced fields due to magnetospheric sources (induced fields due to ionospheric sources are calculated using a 1-D conductivity model, cf. Sabaka *et al.* (2004)). The conductivity model consists of: 1) an inhomogeneous conducting surface shell; 2) three local conductors of 0.04 S/m running from the bottom of that shell down to 400 km depth; 3) a deep-seated regional conductor of 1 S/m below the Pacific Ocean Plate, running from 400 km depth down to 700 km. The local and regional conductors reside in a radially symmetric 1D section which consists of a relatively resistive 400 km upper layer of 0.004 S/m, a 300 km thick transition layer of 0.04 S/m, and an inner uniform sphere of 2 S/m.

The conductance of the surface shell contains contributions from seawater and from sediments. The conductance of the seawater has been derived from the global $5' \times 5'$ NOAA ETOPO map of bathymetry, multiplying the water depth by a mean seawater conductivity of 3.2 S/m. The conductance of the sediments has been derived from the global sediment thickness distribution of Laske and Masters (1997).

Figure 5 shows the various layers of the adopted conductivity model. Conductance of the surface shell (left) varies from tens of S inland up to 35000 S in the oceans. Two local conductors of horizontal size 600×1200 km^2 describe hypothetic plumes under the Baikal rift and under Hawaii (Constable and Heinson, 2004); the third conductor of size 600×3000 km^2 represents a hypothetical subduction zone along the western margin of South America. This part of the model is shown in the middle panel of the Figure. Finally, the right panel shows a deep-seated large scale structure of a hypothetic conductor beneath the Pacific Ocean plate.

The model was discretized in the vertical direction into 4 inhomogeneous spherical sublayers of thickness 1, 150, 250, and 300 km, respectively. Each spherical sublayer was discretized in latitude-longitude direction in 180×90 cells of size $2^\circ \times 2^\circ$.

Magnetospheric primary and induced fields

It is well known that the spatial structure of magnetospheric contributions is more complicated than the field given by a

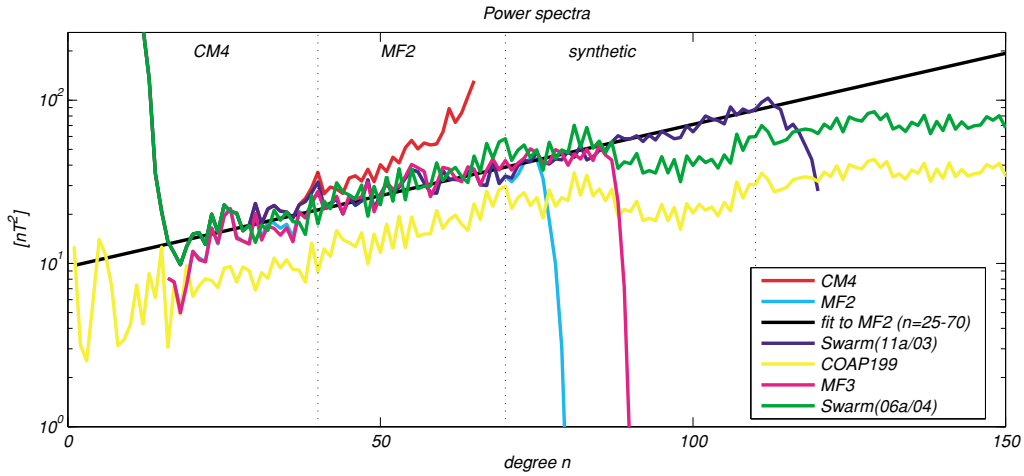


Fig. 3. Power-spectrum of the lithospheric field models used in study.

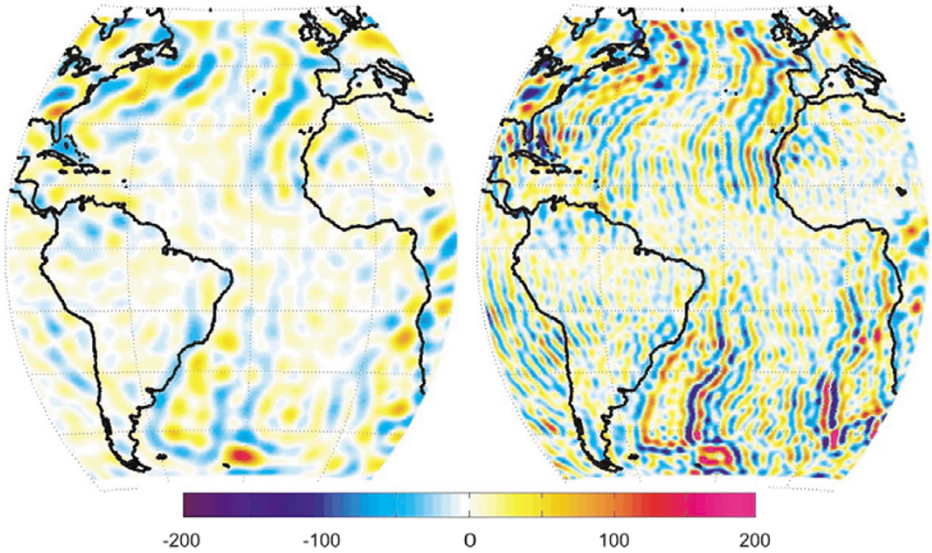


Fig. 4. B_r (in nT) at ground for $n = 15$–60 (present state, left panel) and $n = 15$–130 (*Swarm* result, right panel), as given by the synthetic model swarm(06a/04).

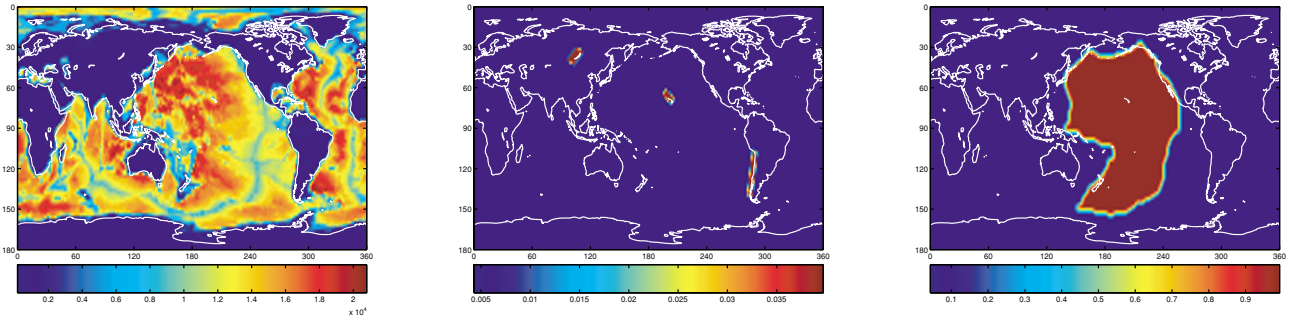


Fig. 5. Left: Surface shell conductance in units of S. Middle: Conductivity [S/m] at depths from 1 km down to 400 km. Right: Conductivity [S/m] at depths from 400 km down to 700 km.

symmetric ring-current in the equatorial plane. Proper description of magnetospheric sources therefore require considering more terms than that of the "P_1^0 hypothesis" widely used in geomagnetic field modeling. Determination of a complicated spatial structure requires, however, multi-point observations, as delivered by *Swarm*. To test the capability of the *Swarm* constellation to unwrap higher magnetospheric terms, a rather sophisticated model of magnetospheric contributions was derived. It is based on an hour-by-hour spherical harmonic analysis of world-wide distributed observatory hourly mean values of the years 1997–2002 in dipole-latitude and magnetic local time. After re-

moval of main field, secular variation and ionospheric (primary and induced) contributions as predicted by CM4 from the observations, a spherical harmonic expansion of the horizontal components is performed and time series of the 9 expansion coefficients of the external potential, $q_n^m(t)$ and $s_n^m(t)$ for $n = 1, \ldots, 3$ and $m = 0, 1$, has been determined. Separation of external and induced fields is done using a 1D model of electrical conductivity. This approach is similar to that described in Olsen and Kuvshinov (2004).

The time series $q_n^m(t), s_n^m(t)$ of the magnetospheric field were then used as input for the calculation of secondary, induced, contributions. The approach consists of the following steps: First, a Fourier analysis of the 5-year time-series is performed and the coefficients $\tilde{q}_n^m(\omega), \tilde{s}_n^m(\omega)$ are obtained, for frequencies between $\frac{1}{5}$ yrs^{-1} and $\frac{1}{2}$ hrs^{-1} (Nyquist frequency). Next, electromagnetic induction simulations are performed in the frequency domain for a subset of logarithmically spaced frequencies (covering $\frac{1}{5}$ yrs^{-1} to $\frac{1}{2}$ hrs^{-1}) using the 3-D model of electrical conductivity (details of the solution can be found in Kuvshinov *et al.* (2002, 2005); Kuvshinov and Olsen (2005)), and for the 9 elementary spherical harmonics of unit amplitude with $n = 1, \ldots, 3$ and $m = 0, 1$, n, m are degree and order of the external (inducing) field. Then the results are spline interpolated in frequency from this coarse subset of frequencies to the "target" frequencies ($f = j/5$ yrs^{-1} $= j/43830$ hrs^{-1}, $j = 1, \ldots, 21915$) to obtain "unit responses" for each frequency and each elementary harmonic (i.e. each degree/order combination, n, m, of the external fields). A spherical harmonic analysis of the "unit response" yields "unit response coefficients" $\gamma_{nk}^{ml}, \eta_{nk}^{ml}$, where the maximum degree/order of the induced field was chosen to $k = 45$. Next, internal, induced, Gauss coefficients $\tilde{g}_k^l(\omega) = \sum_{n,m} \gamma_{nk}^{ml}(\omega)\tilde{q}_n^m(\omega)$ and $\tilde{h}_k^l(\omega) = \sum_{n,m} \eta_{nk}^{ml}(\omega)\tilde{s}_n^m(\omega)$, $k = 1, \ldots, 45$, $l = 0, \ldots, k$, are obtained by multiplying the actual magnetospheric coefficients $\tilde{q}_n^m(\omega), \tilde{s}_n^m(\omega)$ with the unit responses $\gamma_{nk}^{ml}, \eta_{nk}^{ml}$. Fourier transformation yields time series of the induced coefficients $g_n^m(t), h_n^m(t)$ for the whole 5-year period of the simulated mission. Finally, the magnetic components of magnetospheric and induced fields were synthesized at each satellite position from the time series of the coefficients $g_n^m, h_n^m, q_n^m, s_n^m$ after interpolation to the time of the satellite positions. Details can be found in Kuvshinov *et al.* (2006).

Ionospheric primary and induced fields

The primary ionospheric field is described by a spherical harmonic expansion in Quasi-Dipole (QD) coordinates (Richmond, 1995), to take into account the influence of the main field on ionospheric currents. Each coefficient contains daily (24 h, 12 h, 8 h and 6 h) and seasonal (annual and semi-annual) variations. In addition, all coefficients are scaled by daily values of solar flux $F_{10.7}$ (daily values are used to introduce some day-to-day variability of the ionospheric field). Secondary, induced contributions are considered using a 1D model of mantle conductivity. Both ionospheric primary and induced fields are taken from CM4.

Toroidal fields

Toroidal fields are caused by electric currents at satellite altitude. They are taken from CM4 and are based on Ørsted vector data. However, extrapolation from Ørsted altitude (680–850 km) to *Swarm* altitudes turned out to be problematic, especially at the altitude of the lower satellite pair, and therefore the toroidal field has been omitted from most field recovery attempts of the End-to-End simulation study. Since the field contributions to be recovered here are potential fields (which are orthogonal to a toroidal field), omission of the toroidal field is expected to have only minor influence on the recovery of the potential part of the field.

Magnetic fields due to Ocean tides

These are derived for the 10 tidal modes $M_2, S_2, N_2, K_2, K_1, O_1, P_1, Q_1, M_f$ and M_m by calculations that were performed using the models of water transports of TPXO.6.1 (Erofeeva and Egbert, 2002) and a model of electrical conductivity consisting of the inhomogeneous surface shell (cf. Fig. 5, left) and a 1-D mantle underneath. The calculations were performed on a $1^\circ \times 1^\circ$ grid using the scheme described in Kuvshinov and Olsen (2005). Upward propagation from ground to satellite was done using a spherical harmonic expansion up to $n = 45$.

Spacecraft and payload noise

A model of synthetic noise based on CHAMP experience and *Swarm* specifications has been used. We designed random noise that is correlated in time, but uncorrelated among the components (the correlation between components of the present missions Ørsted and CHAMP is dominated by attitude uncertainty, which is expected to be improved significantly for *Swarm*. We therefore believe that the assumption of uncorrelated noise between the components is justified). The standard deviation of the noise is (0.07, 0.1, 0.07) nT for (B_r, B_θ, B_ϕ), in agreement with *Swarm* performance requirements. Comparison of this noise model with the models developed by the two industrial consortia during Phase A of the mission show close agreement, thereby confirming the validity of using the scaled CHAMP spectra for the present study.

2.3 Generation of synthetic data

Magnetic field values have been generated for sampling rates of 1 min (the sampling rate of the synthetic positions) and 5 seconds. The data are provided as daily files containing time, position, and the vector components of the 8 source contributions (from the core, lithosphere, magnetospheric primary and induced field, ionospheric primary and induced fields, toroidal field, and payload noise). In addition, synthetic hourly mean values have been created for 188 observatories and the years 1997–2002. All data are available at the anonymous ftp-server ftp.spacecenter.dk/data/magnetic-satellites/Swarm/E2E/ and we encourage researchers to test their approaches for field modeling and 3-D mantle conductivity recovery using this synthetic data set.

3. Assessment

Several methods have been applied to the synthetic data set in order to recover the various contributions to Earth's magnetic field. In addition to *Comprehensive Inversion (CI)*, two different methods for recovery of the core field and secular variation, two methods for extraction of the high-degree lithospheric fields, and two methods for determining mantle conductivity, have been applied. Details of

these methods and a comparison of the obtained results can be found in Olsen *et al.* (2004).

It turns out that a combination of the results obtained by *CI* (Sabaka and Olsen, 2006) with those of the Gradient method for high-degree lithospheric field recovery (Maus *et al.*, 2006) gave the most promising results. In addition, time series of the magnetospheric field as obtained with *CI* have been used successfully to derive response functions that allow for the detection of 3-D inhomogeneities of mantle conductivity (Kuvshinov *et al.*, 2006).

Before summarizing the obtained results, we want to make a general comment on the difference between single satellite missions and a constellation: Data accuracy of each of the *Swarm* satellites (1 nT of the vector components, 0.3 nT of the field intensity) will be superior to that of any previous and present satellite mission (for which accuracy of the vector components is about 2–5 nT) by at least a factor of 2. The reason for this is the unique triple-head star imager concept in combination with the ultra-stable optical bench that connects star imager and vector magnetometer, and the improved in-flight calibration possibility that the *Swarm* constellation will allow for. This data accuracy improvement will lead to improved magnetic field models. However, probably even more important than the improved *single-satellite* data accuracy is the *constellation concept*, which allows for better separation of the space-time structure of the various magnetic field contributions and thereby better field separation.

Analyzing data from two instead of one satellite will double the number of data points, and from that one might expect an improvement of the results by a factor of $1/\sqrt{2} = 1.41$ (This holds if the data are statistically independent, which is a best case scenario). According to this argument, the combination of data from three satellites would improve the results by a factor of $\sqrt{3} = 1.73$. However, as will be demonstrated now, the actual improvement obtained with the *Swarm* mission is much higher than these values, indicating that advantage has been taken of the constellation during the data analysis.

3.1 Test quantities and criteria

For the assessment of the various satellite constellations and approaches we have used various criteria:

- **Difference in spectra, degree error, and accumulated error**. The Mauersberger-Lowes spectrum (degree variance), R_n, of the differences between the original and the recovered model coefficients, Δg_n^m, Δh_n^m, in combination with the spectrum of the original model, has been used to evaluate a recovered model. Degree error is defined as $\sqrt{R_n}$, and accumulated error at degree n is defined as $\sqrt{\sum_{l=l_{\min}}^{n} R_l}$.
- **Degree correlation**, ρ_n, (Langel and Hinze, 1998, eq. 4.23) between the original and the recovered model has also been used to evaluate a recovered model. Models are considered compatible up to that degree n where ρ_n drops below 0.7.
- **Sensitivity matrix** is the relative error of each coefficient in a degree versus order matrix and was used to investigate systematic errors. The difference (recovered minus original model) of all the coefficients is determined and subsequently normalized by the mean spectral amplitude of the associated degree n.
- Finally, **global maps** of field differences (for instance of B_r) between the original and the recovered model are used to find geographically confined deficiencies in the recovered models, for instance in connection with the size of the polar gaps.

3.2 Performance related to lithospheric field

The aim of the mission is to determine global lithospheric models with details corresponding to spherical harmonic degree up to 110 or higher such that the signal to noise ratio for the degrees of the estimated model is still larger than one. This will allow narrowing or closing the spectral gap existing between the global models and the regional surveys.

The black curve of the left panel of Fig. 6 shows the degree signal (i.e. the square root of the degree variance) of the lithospheric field at ground, as given by the synthetic model swarm(06a/04). The degree errors of models derived from Magsat and CHAMP combined with Ørsted, are shown by dashed blue curves. (The error of the Magsat model is found from the difference between MF3 and a Magsat model derived by Cain *et al.* (1985); that of the CHAMP model is found from the difference between MF3 and CM4). The error exceeds the signal beyond degree 30 for Magsat and beyond degree 60 for the present CHAMP model. The difference between CHAMP and Magsat models is due to significantly improved data accuracy and due to the longer observational period. Future CHAMP data collected at 300 km altitude will probably allow extending this model to degree 70 or so.

The magenta curve shows the error of a model derived from single *Swarm* satellite data obtained at an altitude of about 300 km towards the end of the mission. Compared to present state-of-the-art models, this curve indicates the improvement that one will get from the higher accuracy of the single satellite *Swarm* data. Combining data from the two side-by-side flying lower *Swarm* satellites A and B provides a significantly improved field recovery at higher degrees. These results have been obtained by Maus *et al.* (2006) using the Gradient method.

The green curve shows the three-satellite solution (*Swarm* A, B and C). This optimal three-satellite model is obtained by combining the results of the *CI* (Sabaka and Olsen, 2006) for $n < 83$ and of the Gradient method (Maus *et al.*, 2006) for $n = 84$–140.

Co-estimation of external and induced fields results in much improved lithospheric field recovery for degrees below 80. Adding data from the fourth satellite, *Swarm D*, (yellow curve) does not improve lithospheric field recovery significantly.

Figure 7 presents an assessment of the optimal 3-satellite solution as measured by various test criteria. The spectrum of the difference between the original and the recovered model is smaller than the crustal signal for degrees up to $n = 130$ (upper left), and degree correlation $\rho_n > 0.7$ for $n < 130$ (lower left). The sensitivity matrix (lower right) indicates enhanced high-degree error for the zonal ($m = 0$) coefficients for $n > 80$.

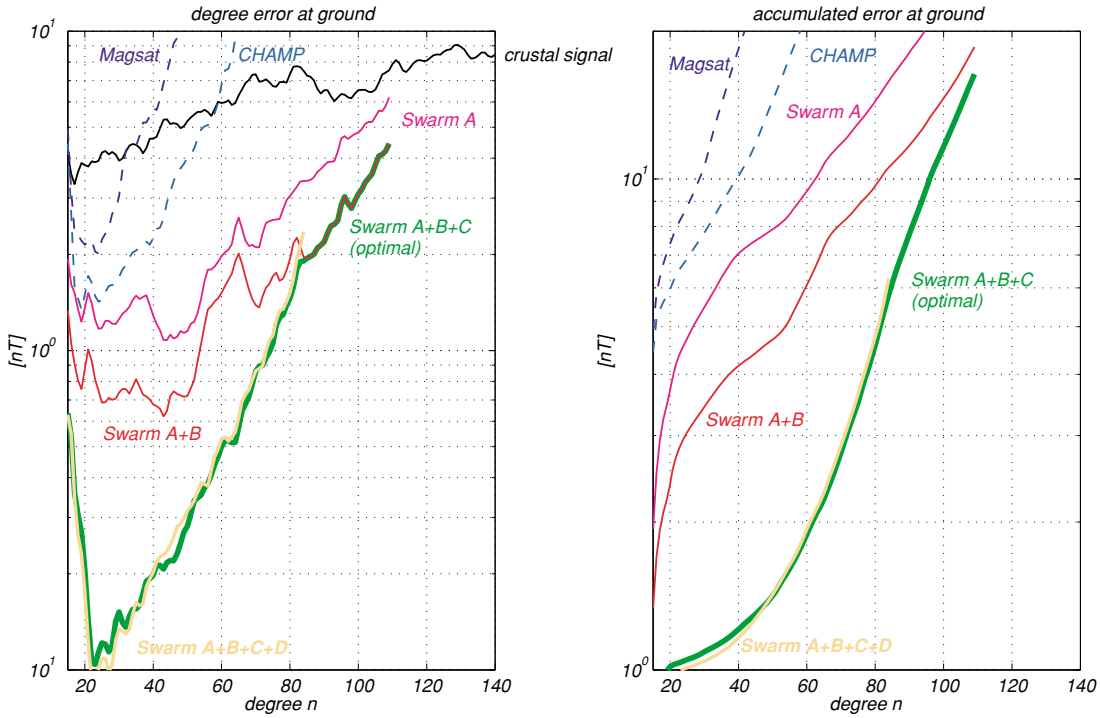


Fig. 6. Left: Degree error (at the Earth's surface) of the lithospheric field recovery for different satellite combinations and approaches. Black curve presents lithospheric signal as given by the synthetic model swarm (06a/04). Right: accumulated error, i.e. the square root of the sum (from degree 14 to n) of the degree variances.

3.3 Performance related to core field and secular variation

Combining existing Ørsted, CHAMP and future *Swarm* observations will more generally allow any magneto-hydrodynamic phenomena affecting the core on sub-annual to decadal scales to be investigated, down to length scales of about 2850 km or spherical harmonic degree 14. This requires a model of secular variation to be estimable up to the same degree with signal to noise larger than one for degree 14.

No other satellite missions are presently planned for the years after 2010. Hence without *Swarm* satellite data, models of the time change of the magnetic field at the beginning of the next decade have to be based on magnetic observatory data. This allows for deriving field models only up to degree 7 or 8 Alexandrescu *et al.* (1994); Lesur *et al.* (2006), indicated by the magenta line in Fig. 8. Models derived from single-satellite missions will reduce the degree error typically by one order of magnitude. The proposed constellation with 3 *Swarm* satellites allows determining secular variation models up to degree 15, with half the degree error obtainable with a single satellite. This result has been found by means of the *CI* approach (Sabaka and Olsen, 2006).

3.4 Performance related to 3-D mantle conductivity

Magnetic field variations with periods of a few hours to 30 days sense mantle conductivity in the depth range between about 200 and 1000 km. *Swarm* will for the first time allow for a global determination of 3D structures in the electrical conductivity of the mantle, as has been demonstrated by Kuvshinov *et al.* (2006). The key for this is the simultaneous observation of the magnetic field variations at different local times, resulting in models of the time-space structure of inducing magnetospheric fields. This can be achieved down to a horizontal scale of 8000 km, corresponding to spherical harmonic degree 5, using magnetic observations in the period range of a few days.

The C-response (Schmucker, 1985) of a location is a transfer function that connects the vertical component of the magnetic field variation and the horizontal derivatives of the horizontal components; its frequency dependence contains information on the variation of conductivity with depth in the surrounding of that location. The real part of the C-response indicates the depth of the induced currents; regions with reduced real parts indicate shallower induced currents. This is demonstrated in the left part of Fig. 9, which shows the true value of the real part that has been used as input for the simulation. The center part of the figure demonstrates a successful detection of a conductivity anomaly beneath the Pacific with 3 *Swarm* satellites; a detection using single satellites (right panel) is not possible. C was derived using time series of magnetospheric and induced spherical harmonic expansion coefficients that were derived using *CI*; see Kuvshinov *et al.* (2006) and Sabaka and Olsen (2006) for details.

This demonstrates the ability of *Swarm* to detect a region of enhanced conductivity at 400 km depth, the boundary of which is indicated by the thick black line. External field variations of 7-day period induce currents, the center of which is normally at about 800–900 km depth. The currents will, however, flow at shallower depth beneath the Pacific, since they tend to flow in regions of higher conductivity.

Three specific locations, marked in green in Fig. 9, are selected, because they represent different regimes for the mantle environment. The frequency-dependence of the C-

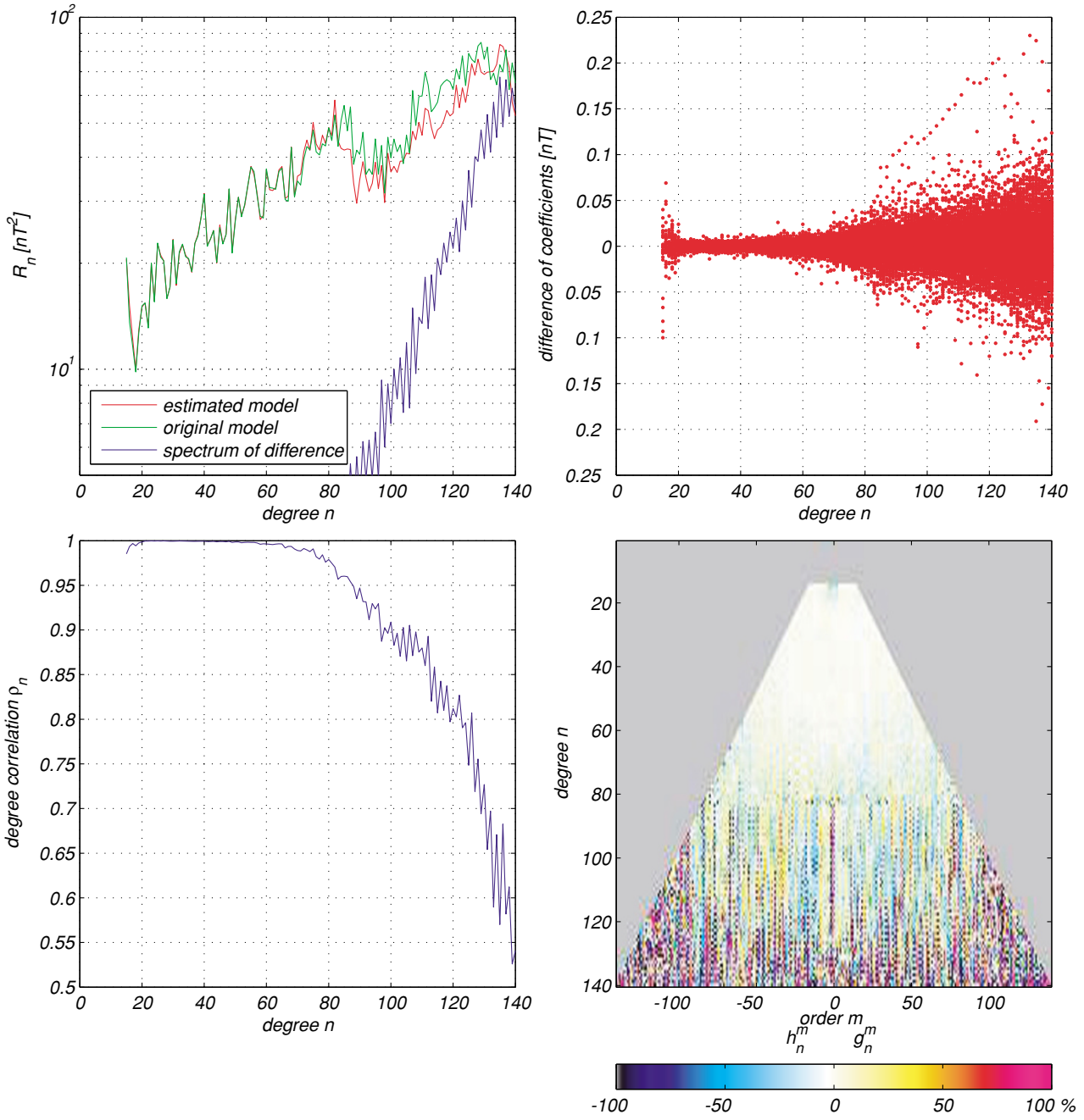


Fig. 7. Quality of the optimal 3-satellite solution. True and retrieved signal spectrum, plus error spectrum (*upper left*); absolute error of Gauss coefficients (*upper right*); degree correlation between input and retrieved lithospheric magnetic field model (*lower left*); sensitivity matrix (*lower right*). Cf. Subsection 3.1 for a definition of these quantities.

response for these locations is shown in the left part of Fig. 10; as expected, the real part increases with period, since variations at longer periods penetrate deeper into the mantle. The right panel shows the error in the recovered C-response from 1 and 3 satellites, respectively. The recovery is shown in relation to the original model responses for these locations in Fig. 9. The relative errors in the right panel of this figure show a drastic improvement for three satellites, of approximately 10–20% of the expected responses, whereas the single-satellite solutions perform poorly. Since the model does not contain inhomogeneities in the lower mantle, the error of the single satellite solution is less at longer periods, but still larger than that of the three-satellite solution by a factor of at least 2.

3.5 Performance summary

The main findings related to the primary objectives for retrieving lithospheric and secular variation models are summarized in Table 2. If the magnetic field product requirements are met for each satellite (which follows from the error assessment of the industrial feasibility studies during Phase A of the project), the proposed three satellites constellation will lead to a drastic improvement in the derived models. The relative improvement, which would be achievable by adding a fourth satellite appears to be marginal in relation to these objectives. However, specific scientific investigations related to the external field could benefit from

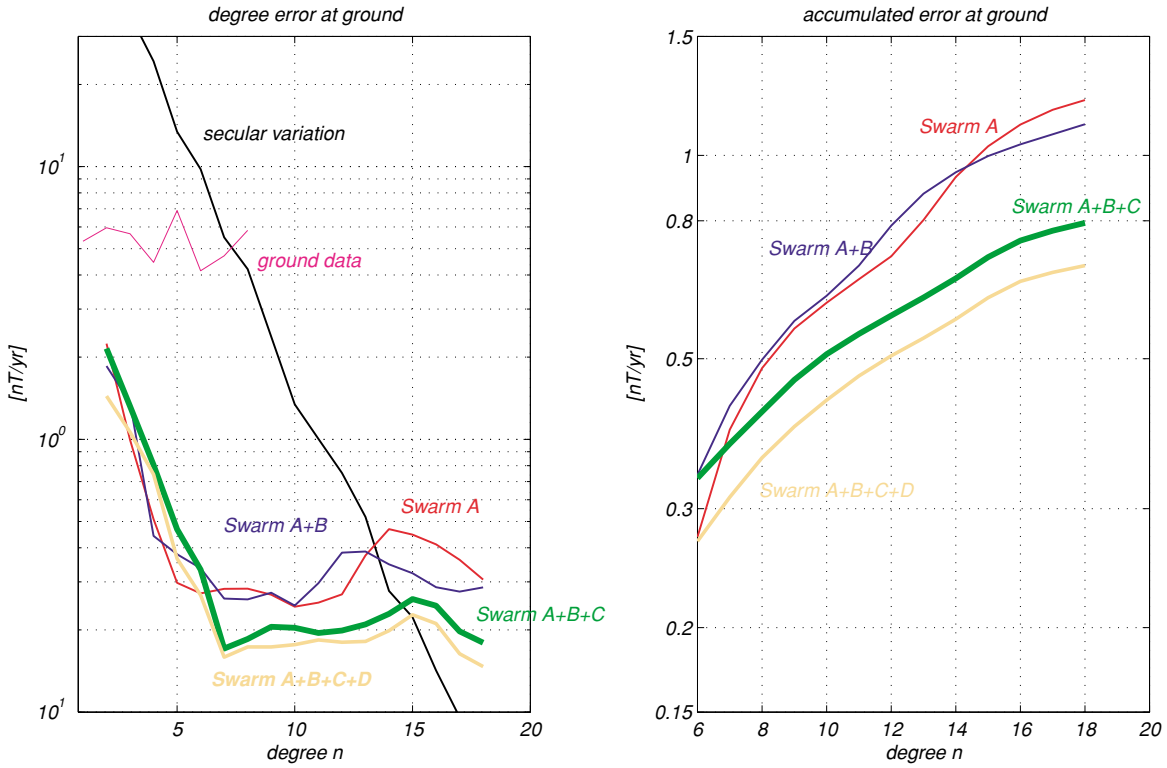


Fig. 8. As Fig. 6, but for the secular variation. The magenta line represent the error of a model that has been estimated using simulated observatory data only (Lesur *et al.*, 2006).

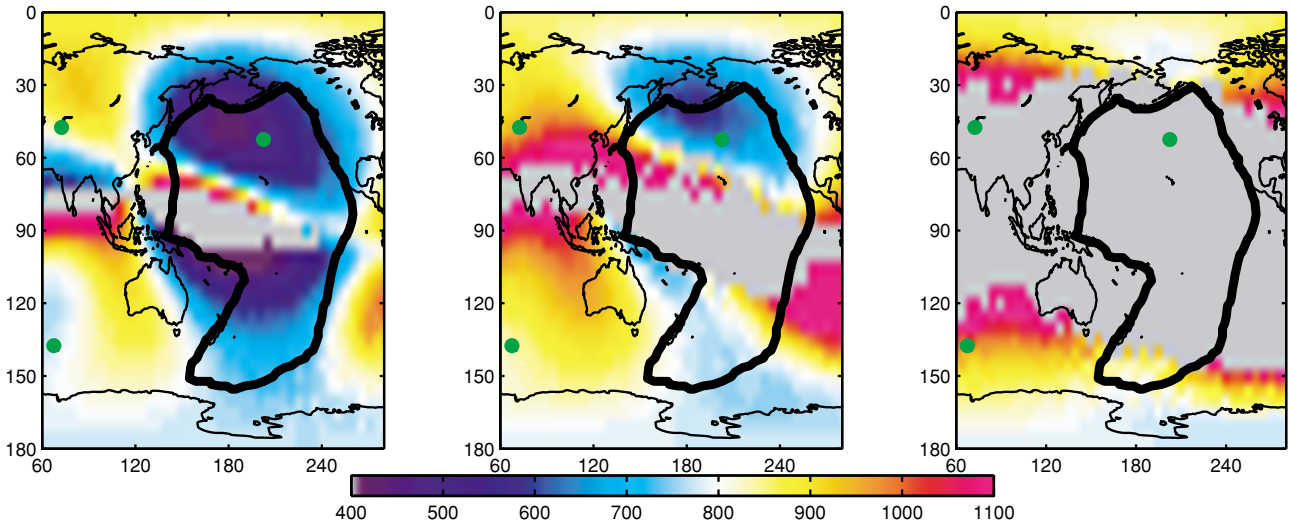


Fig. 9. Maps of the real part of the C-response (in km) for a period of 7 days. The thick black curve indicates the boundaries of a hypothetic conductivity anomaly at 400 km depth. True values (left); estimated ones using 3 satellites (center); and estimated ones from one single satellite (right). Regions in which squared coherency is below 0.6 are excluded and shown in grey.

such a fourth satellite, but this was not the topic of the present study. The error statistics and quality measures are shown in Table 2 for the estimated lithospheric and secular variation models from ground data only, from a single lower satellite (A), from the lower satellite pair (A+B), from the three satellite constellation (A+B+C, see Fig. 1) and from the four satellite constellation. This complements the spectral plots in Figs. 6, 7 and 8. The performance is expressed at or up to the degree ($n = 60$) where CHAMP lithospheric model errors and where errors in the SV model ($n = 8$) from observatory data start to dominate over the signal. The values are given at the Earth's surface ("at ground") and at satellite level to illustrate the effect of downward continuation and the size of the model error at satellite altitude ("at 400 km altitude"). The indicators used to express the performance results are (see also Section 3.1):

- **degree error:** is the standard deviation of the error for a degree (cf. the left parts of Figs. 6 and 8),

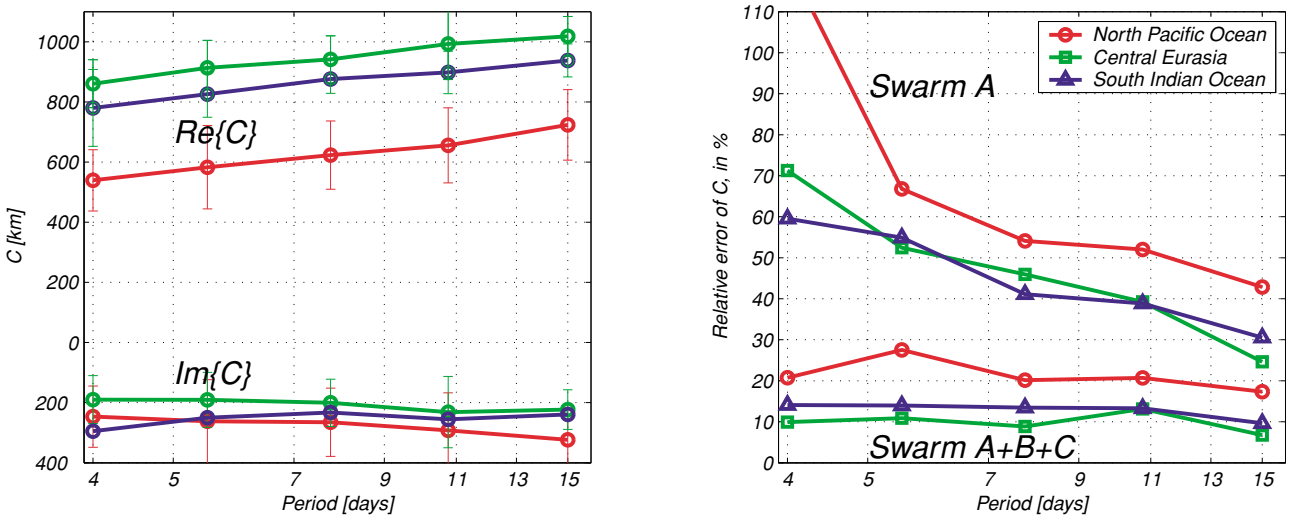


Fig. 10. Left: Single site C-response estimation using 3 satellites against true values and error bars. The locations of these sites are shown by the green dots in Fig. 9. Right: The relative error of C-response estimation at those sites, obtained from a single satellite (*Swarm A*) and from the proposed 3 satellites constellation (*Swarm A+B+C*).

Table 2. Expected performance related to primary objectives of the mission.

			without *Swarm**	1 satellite (A)	2 satellites (A+B)	3 satellites (A+B+C)	4 satellites (A+B+C+D)
Lithospheric Field	At ground	Degree error, n=60 [nT]	6.8	2.0	1.5	0.50	0.50
		Accumulated error, n=14-60 [nT]	23.2	11.3	8.5	2.0	2.0
		Degree error, n=110 [nT]	N/A	6.3	4.4	4.4	4.4
		Accumulated error, n=14-110 [nT]	N/A	29	20	16	16
	At 400 km altitude	Degree error, n=110 [nT]	N/A	0.0072	0.0052	0.0052	0.0052
		Accumulated error, n=14-110 [nT]	3.80	2.91	2.58	0.41	0.39
	altitude independent	Relative error, n=60 [%]	117	34	26	4.1	4.1
		Degree correlation, n=60	0.58	0.94	0.97	0.996	0.996
		Relative error, n=110 [%]	N/A	67	47	47	47
		Degree correlation, n=110	N/A	0.74	0.87	0.88	0.88
Secular Variation	At ground	Degree error, n=8 [nT/yr]	2.3	0.28	0.26	0.18	0.17
		Accumulated error, n=6-8 [nT/yr]		0.52	0.50	0.42	0.36
		Degree error, n=14 [nT/yr]	N/A	0.47	0.35	0.22	0.20
		Accumulated error, n=6-14 [nT/yr]	N/A	0.99	0.94	0.65	0.57
	At 400 km altitude	Degree error, n=14 [nT/yr]		0.176	0.132	0.086	0.075
		Accumulated error, n=6-14 [nT/yr]	N/A	0.47	0.45	0.34	0.30
	Altitude independent	Relative error, n=8 [%]	32	6.7	6.2	4.4	4.1
		Degree correlation, n=8		0.996	0.998	0.999	0.999
		Relative error, n=14 [%]	N/A	168	126	82	71
		Degree correlation, n=14	N/A	0.59	0.69	0.80	0.82

*The lithospheric results listed in the column labeled "without *Swarm*" are based on present day models (CHAMP and Ørsted); the secular variation results are based upon the ground observatory network available at the time of *Swarm*.

- **accumulated error:** is the standard deviation of the error for the range of spherical harmonic degrees that are included in the model: the commission error (cf. the right parts of Figs. 6 and 8)
- **relative error:** for a certain degree the sum over all orders of differences between estimated and true model coefficients divided by the true model values and converted into a percentage,
- **degree correlation:** correlation coefficient for a certain degree.

The first two indicators give an impression of the standard deviation of the error at today's resolution and target resolution for *Swarm*. The accumulated error is the model commission error that can be taken into account when combining the model with regional data to add the details to the model. The errors of the latter need to be propagated and

combined with those of the satellite model to get a total error of the refined model. For example the global lithospheric model derived from three satellites has a standard deviation of the error of 16 nT, on average globally and at ground, for all details down to about 360 km ($n = 110$). The last two indicators basically show the relative size of the error compared to the signal at a degree and the correlation indicates how alike the shape of the estimated signal and the true model are. So, a relative error below 100% leaves room for estimating models to even higher spherical harmonic degree. From the analysis of the results for three satellites it appears possible to recover the signals up to the finest scales, which is necessary to achieve the research goals for *Swarm*. Overall, the analysed three-satellite constellations meet the *Swarm* requirements, while the two-satellite performance does not.

4. Conclusions

The experience gained from the existing missions and the extensive detailed scientific studies of various constellation scenarios, performed during Phase A of *Swarm*, have very convincingly demonstrated that a dedicated mission like *Swarm* will bring significant advances in many science fields from the deep core to the external environment of the Earth. The constellation concept of *Swarm* allows a much better separation of different magnetic field contributions, and will furthermore provide measurements that can be used for completely new investigations and methodology developments.

Acknowledgments. The *Swarm* End-to-End Mission simulation study has been funded by ESA through contract No. 17263/03/NL/CB. NASA has supported the study under Contract NAS5-00181. We'd like to thank Eigil Friis-Christensen, Gauthier Hulot, Hermann Lühr, Monika Korte, Susan Macmillan, Franz-Heinrich Massmann, Jean-Claude Raimondo, Patricia Ritter, Pascal Tarits and Alan Thomson for their contribution to this study.

References

Alexandrescu, M., C. H. Duyen, and J.-L. LeMouel, Geographical distribution of magnetic observatories and field modelling, *J. Geomag. Geoelectr.*, **46**, 891–901, 1994.

Cain, J. C., D. R. Schmitz, and L. Muth, Small-scale features in the Earth's magnetic field observed by MAGSAT, *J. Geophys. Res.*, **89**, 1070–1076, 1985.

Constable, S. and G. Heinson, Hawaiian hot-spot swell structure from seafloor MT sounding, *Tectonophysics*, **389**, 111–124, 2004.

Dyment, J. and J. Arkani-Hamed, Contribution of lithospheric remanent magnetization to satellite magnetic anomalies over the world's oceans, *J. Geophys. Res.*, **103**, 15,423–15,442, 1998.

Erofeeva, S. and G. Egbert, Efficient inverse modelling of barotropic ocean tides, *J. Ocean. Atmosph. Technol.*, **19**, 183–204, 2002.

Fox Maule, C., M. Purucker, and N. Olsen, The magnetic crustal thickness of Greenland, in *Earth Observation with CHAMP, Results from Three Years in Orbit*, edited by C. Reigber, H. Lühr, P. Schwintzer, and J. Wickert, Springer Verlag, 2005.

Friis-Christensen, E., H. Lühr, and G. Hulot, *Swarm*—a constellation to study the dynamics of the Earth's magnetic field and its interactions with the Earth system, DSRI Report 1/2002, Danish Space Research Institute, Copenhagen, 2002.

Friis-Christensen, E., H. Lühr, and G. Hulot, *Swarm*: A constellation to study the Earth's magnetic field, *Earth Planets Space*, **58**, this issue, 351–358, 2006.

Haagmans, R., A synthetic Earth for use in geodesy, *J. Geodesy*, **74**, 503–511, 2000.

Kuvshinov, A. V. and N. Olsen, 3D modelling of the magnetic field due to ocean flow, in *Earth Observation with CHAMP, Results from Three Years in Orbit*, edited by C. Reigber, H. Lühr, P. Schwintzer, and J. Wickert, Springer Verlag, 2005.

Kuvshinov, A. V., D. B. Avdeev, O. V. Pankratov, S. A. Golyshev, and N. Olsen, Modelling electromagnetic fields in 3D spherical Earth using fast integral equation approach, in *3D Electromagnetics*, edited by M. S. Zhdanov and P. E. Wannamaker, chap. 3, pp. 43–54, Elsevier, Holland, 2002.

Kuvshinov, A. V., H. Utada, D. Avdeev, and T. Koyama, 3-D modelling and analysis of Dst C-responses in the North Pacific ocean region, revisited, *Geophys. J. Int.*, **60**(2), 505–526, doi: 10.1111/j.1365–246X.2005.02,477.x, 2005.

Kuvshinov, A. V., T. Sabaka, and N. Olsen, 3-D electromagnetic induction studies using the *Swarm* constellation: Mapping conductivity anomalies in the Earth's mantle, *Earth Planets Space*, **58**, this issue, 417–427, 2006.

Langel, R. A. and W. J. Hinze, *The Magnetic Field of the Earth's Lithosphere: The Satellite Perspective*, Cambridge University Press, 1998.

Laske, G. and G. Masters, A global digital map of sediment thickness, *EOS Trans. AGU*, **78**, F483, 1997.

Lesur, V., S. Macmillan, and A. Thomson, Deriving main field and secular variation models from synthetic Swarm satellite and observatory data, *Earth Planets Space*, **58**, this issue, 409–416, 2006.

Maus, S., M. Rother, R. Holme, H. Lühr, N. Olsen, and V. Haak, First scalar magnetic anomaly map from CHAMP satellite indicates weak lithospheric field, *Geophys. Res. Lett.*, **29**, 2002.

Maus, S., M. Rother, K. Hemant, H. Lühr, A. V. Kuvshinov, and N. Olsen, Earth's crustal magnetic field determined to spherical harmonic degree 90 from CHAMP satellite measurements, *Geophys. J. Int.*, 2005 (submitted).

Maus, S., H. Lühr, and M. Purucker, Simulation of the high-degree lithospheric field recovery for the Swarm constellation of satellites, , High degree lithospheric field recovery, *Earth Planets Space*, **58**, this issue, 397–407, 2006.

Nataf, H. and Y. Ricard, 3SMAC: an a priori tomographic model of the upper mantle based on geophysical modeling, *Physics of the Earth and Planetary Interiors*, **95**, 101–122, 1996.

Olsen, N. and A. V. Kuvshinov, Modelling the ocean effect of geomagnetic storms, *Earth Planets Space*, **56**, 525–530, 2004.

Olsen, N., *et al.*, *Swarm*—End-to-End mission performance simulator study, ESA contract No 17263/03/NL/CB, DSRI Report 1/2004, Danish Space Research Institute, Copenhagen, 2004.

Purucker, M. E. and J. Dyment, Satellite magnetic anomalies related to seafloor spreading in the South Atlantic Ocean, *Geophys. Res. Lett.*, **27**, 2765–2768, doi:10.1029/1999GL008,437, 2000.

Richmond, A. D., Ionospheric electrodynamics using magnetic Apex coordinates, *J. Geomag. Geoelectr.*, **47**, 191–212, 1995.

Ritter, P. and H. Lühr, Curl-B technique applied to *Swarm* constellation for determing field-aligned currents, *Earth Planets Space*, **58**, this issue, 463–476, 2006.

Sabaka, T. J. and N. Olsen, Enhancing comprehensive inversions using the *Swarm* constellation, *Earth Planets Space*, **58**, this issue, 371–395, 2006.

Sabaka, T. J., N. Olsen, and R. A. Langel, A comprehensive model of the quiet-time near-Earth magnetic field: Phase 3, *Geophys. J. Int.*, **151**, 32–68, 2002.

Sabaka, T. J., N. Olsen, and M. Purucker, Extending comprehensive models of the Earth's magnetic field with Ørsted and CHAMP data, *Geophys. J. Int.*, **159**, 521–547, doi: 10.1111/j.1365–246X.2004.02,421.x, 2004.

Schmucker, U., Magnetic and electric fields due to electromagnetic induction by external sources, in *Landolt-Börnstein, New-Series, 5/2b*, pp. 100–125, Springer-Verlag, Berlin-Heidelberg, 1985.

Seeber, G., *Satellite Geodesy*, Walter de Gruyter, Berlin-New York, 2004.

N. Olsen (e-mail: nio@spacecenter.dk), R. Haagmans, T. J. Sabaka, A. Kuvshinov, S. Maus, M. E. Purucker, M. Rother, V. Lesur, and M. Mandea